

WING STATIC STRUCTURAL ANALYSIS AND EXPERIMENTAL TESTING OF A COMPOSITE 1:8 S55-X REPLICA

G.Nicolosi¹, A.Lunghitano¹, S.Lombardi¹, T.Talamucci¹, A.Caivano¹, N.Simone¹
&
E.Cestino¹, V.Sapienza²

¹ Department of Mechanical and Aerospace Engineering, Politecnico di Torino, Turin, Italy

²Aeronautical Engineering Consultant, Turin, Italy

Abstract

An aircraft structure should be designed in order to satisfy the stiffness and strength requirements. In this study, a seaplane model, made by carbon fiber, has been selected to analyze the wings' load capability, deflection and to verify that the structure, up to limit loads, has been designed according to regulatory requirements. The whole process is supported by various numerical analyses, including the FEM analysis, to verify the aircraft's behavior when subjected to a 4g pull-up maneuver. Experimental wing static tests were planned and carried out to compare the results of this analysis and to show displacements and strains of the aircraft's structure analyzed.

Keywords: Wing static test, Composite materials, FEM, Seaplane, Aircraft structure

1. Introduction

"Team S55" is a team from "Politecnico di Torino" whose purpose is to build a 1:8 scale replica of "Savoia-Marchetti S55-X" [1][2], a seaplane produced in Italy in the 1920s. Firstly, it has been studied the historical model, optimizing it with the current knowledge and resources in collaboration with external engineering experts.

The structure has to withstand the aerodynamic and inertial loads expected during the maneuver conditions. As required by CS25.301 and CS23.305 [3][4], the wing must sustain the Limit Load "LL", which is the maximum load expected in all the flight envelope without showing permanent damages or deformations after load removal. Additionally, the seaplane must resist for at least three seconds without collapsing to the Ultimate Load ("UL"), obtained by increasing the LL by a Safety Factor ($n=2$). In the interest of verifying these requirements, a static test was designed [5]. A longitudinal maneuver is considered to create a wing load compatible with a load factor condition $N_z=4$.

In order to advance the test results, a finite element static analysis was carried out in three steps: pre-processing, processing, and post-processing. In the first step, data about materials' properties, geometry and mesh, load cases, and constraints are collected; in the second one, calculations of items are performed, such as stiffness matrix, nodal forces vector, unconstrained degrees-of-freedom, and surface forces. In the last step, the calculation via FEM of deflection and stress was done.

The first and the last steps were performed through ANSA and META respectively, both from BETA CAE Systems, while the processing step was performed via NASTRAN from MSC.

Simulations are compared to an experimental test: deflections and deformations are measured in different load cases.

The test should have been executed using a lever system in order to simulate the load's distribution, as described in the 4th chapter, but a simplified version of the test was designed and tested experimentally to follow a strict roadmap. This version replaced the distributed load with a point load placed on a singular rib per half-wing.

The complete test has been wholly developed, but it has not been executed yet.

2. FEM Analysis

The structural analysis was made using the Finite Element Method via ANSA code: firstly, a CAD file was imported into ANSA. Through the Mesh operation, the structure can be simplified into small finite elements that are easier to handle; this task can be fulfilled in ANSA running the *Batch Mesh* tool.

Figure 1 shows ANSA's model of the analyzed aircraft structure.

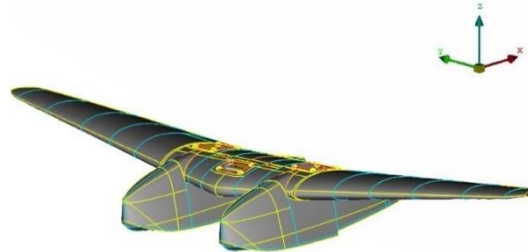


Figure 1 - ANSA model

The structure was made of carbon fiber, 6061 Aluminum alloy, and PVC. In Table 1 each material, its properties, and its application are listed:

| Material | FEM Type Material | Longitudinal Young modulus E1 (MPa) | Transversal Young modulus E2 (MPa) | Poisson's ratio nu12 | Shear modulus G12 (MPa) | Density rho (g/cm ³) |
|-----------------------------|-------------------|-------------------------------------|------------------------------------|----------------------|-------------------------|----------------------------------|
| 6061 Aluminium alloy | MAT1 | 69000 | | 0.33 | 26000 | 2.976 |
| Carbon fiber | MAT8 | 130000 | 10300 | 0.25 | 6500 | 1.857 |
| PVC | MAT6 | 1 | 1 | 0.30 | | 1.400 |

Table 1 - Material properties

A brief description of the main items from the structural point of view is shown below. All the parts were created via *PSHELL* → *laminare* tool: it defined the membrane, bending, and shear properties of shell elements. To simplify the simulations, each single twill layer was replaced by two unidirectional layers. Figure 2 shows the main and secondary spars, both tapered. The middle part of the anterior spar was made up of ten carbon fiber twill layers, each one 0.250 mm thick and characterized by a 0°/90° fibers inclination in the direction of the wingspan and in the flight direction respectively.

The spars were made up of the same carbon fiber material. They are represented in Figure 2 and their properties are listed in Table 2.

| Spar | Material | N° of twill layers | Layer thickness (mm) | Fiber orientation |
|-------------------------|--------------|--------------------|----------------------|-------------------|
| Main center spar | Carbon fiber | 10 | 0.25 | 0°/90° |
| Main Wing spar | Carbon fiber | 12-10-8-6 | 0.25 | 0°/90° |
| Secondary spar | Carbon fiber | 4-6 | 0.25 | 0°/90° |

Table 2 - Spars' properties

In relation to the ribs shown in Figure 2 they were made up by a single sandwich panel with a 5 mm PVC core between two 0.250 mm thick carbon fiber faces. The following figures are shown in half structure for simplicity, considering the symmetry of the model.

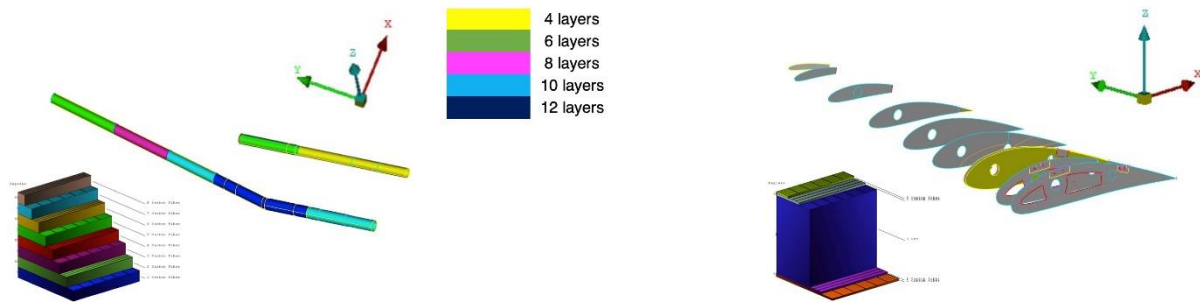


Figure 2 - Main and secondary spars and the middle part lamination of the posterior spar displayed on the left. Ribs and their lamination on the right.

Both wing's skin and shelf's skin, as shown in Figure 3, were composed by four carbon fiber twill layers 0.250 mm thick 45°/-45° fiber-orientated.

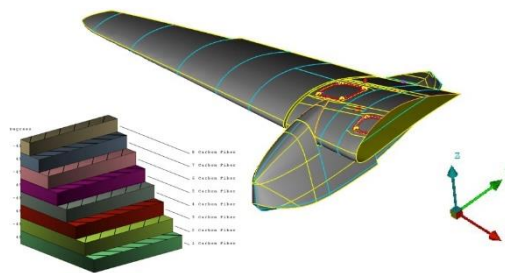


Figure 3 – Shelf, hull and wing skin. Lamination displayed

The hull's skin, as in Figure 3 was composed of four carbon fiber twill layers for a 1 mm total thickness. Interfaces with wing and tail booms are made by Aluminum. Ribs contained in the hull were the same as the wing's ones; thus, they had got the same properties. A number of RBE2 elements were used to virtually recreate a rigid joint to equally deliver the payload between the parts. The boundary conditions were recreated using the ANSA SPC tool and the Distribute FORCES tool.

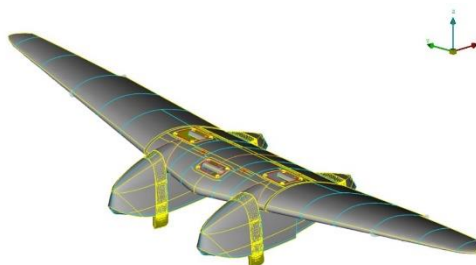


Figure 4 - Payload and constraint's configuration

Some wooden saddles were used to support the ribs of wing structure in the static test where the loads are applied by 4 belts in the front and rear part of each hull. The same constraints and loading were simulated by FEM, as shown in Figure 4.

G – force was not considered because it has been excluded during the experimental analysis through the sensors' calibration.

Lastly, a linear static analysis was performed to evaluate the deflection of the structure under the influence of all forces and constraints. This analysis was accomplished through the proper ANSA' *Nastran Header* → *sol101* tool.

3. Simplified experimental test

The simplified experimental test was designed in preparation for the final test, that was executed later. The process aimed to verify the reliability of the structural analysis to predict the deflection of the wing. Firstly, it is necessary to define the structure composed by the Test Article and the Test Arrangement.

3.1. Test Article definition

The Test Article, see in Figure 5, was the body that includes the main components of the seaplane: complete wing, central wing box, and hulls; it is the structure to be examined during the test. Special care is required in managing these components to avoid any structural damage.

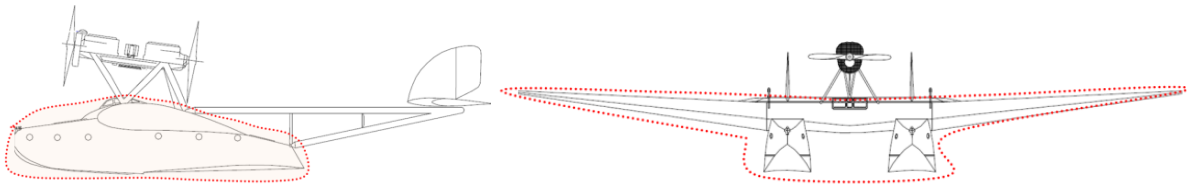


Figure 5 - The Test Article

3.2. Test Arrangement definition

The wing was installed on the Test Arrangement that allowed a proper load application and provided for the equilibrating reaction of the fuselage structure. It included two supports whose height was 1.65 meters; each half-wing was positioned to one support at the fourth rib, Figure 6. This point was chosen for the presence of the spar and because it did not interfere with the operations of the aileron.

Each of the supports had a wooden saddle on top, with a rubber strip that fitted the lower part of the fourth rib's profile to avoid damage to the skin.



Figure 6 - Support of the half wing

3.3. Instrumentation

3.3.1. Sensors

LVDT sensors shown in Figure 7 were used throughout the experiment to measure the displacement in eight positions of the Test Article. The transducers' characteristics are in Table 3:

| Transducer type | | WI/10mm-T |
|--|----------------|-----------|
| Nominal (rated) displacement (nominal (rated) measuring span) | mm | 10 |
| Nominal (rated) output span (between starting point and endpoint when output is not under load) | $\frac{mV}{V}$ | 80 |
| Nominal (rated) signal at starting point | $\frac{mV}{V}$ | -40 |
| Nominal (rated) signal at endpoint | $\frac{mV}{V}$ | 40 |
| Nominal (rated) output span tolerance | % | ±1 |
| Zero signal setting tolerance | $\frac{mV}{V}$ | ±4 |
| Linearity deviation (max. deviation between starting point and endpoint, including hysteresis) | % | 0,2 |
| Weight of measuring element without connection cables | g | 20 |
| of moving parts | g | 5.5 |

Table 3 - LVDT datasheet



Figure 7 - LVDT

Output usually corresponds to zero signal when the plunger is at half of the measuring range, but other definitions can be given for this signal.

Transducers were connected to an acquisition system HBM QuantumX MX840B in Figure 8.



Figure 8 - Acquisition System

The device has eight acquisition channels. Furthermore, the device transferred the collected data to Catman software to process the results.

3.3.2. Loading system

The loading system comprised two plates and two belts and some masses that were gradually added. Both belts wrapped the hulls, and the plates were hung on them.

| Components | | Weight [Kg] | Photo |
|------------------|-------|-------------|--|
| Test Article | | 13,36 |  |
| Plates and belts | Right | 8,60 |  |
| | Left | 8,42 | |

Table 4 - Test article and load instrumentation weights

3.4. Procedure

LVDT transducers were positioned on a horizontal plane, which guaranteed a right angle with the ground, to be in contact with the belly of the wing and the hulls in correspondence with the measurement points. They measure displacements in one direction: in this case, the z-axis was chosen (also called “height axis”). The placements of the transducers are shown in Table 5:

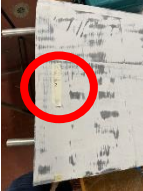
| 1 | 2 | 3 | 4 |
|--|--|---|--|
| Central wing box (symmetry plane) | Half wing | Left hull (trailing edge) | Left hull ($\frac{2}{3}$ of the hull's chord) |
|  |  |  |  |
| 5 | 6 | 7 | 8 |
| Right hull (trailing edge) | Left hull ($\frac{1}{3}$ of the hull's chord) | Saddle | Saddle |
|  |  |  |  |

Table 5 - LVDT positions on the bottom face of the seaplane

The sensors 7 and 8 measured the compression of the supports' rubber. Every transducer was supported by a rod which was suitably adjusted in height for each point.



Figure 9 – Test set-up

As soon as the equipment was placed, the loading procedure began, as shown in Figure 9. Several steps were taken, each consisting of the loading of some weight: masses were located on plates, and after a few seconds, HBM Catman software elaborated data for each loading step. The test ended when the limit load was reached at about 100 kg.

4. Results: numerical and experimental method comparison

The phenomenon should be studied with a continuously increased load, which was distributed on the seaplane wings. Although, the chosen practical solution was to apply a local force on the two hulls to make a staircase load with a step of 10 kg. First, the seaplane, the ropes, and the load plates were weighted to evaluate the unloaded configuration.

| | | Loading phase | | | | | | FEM Results | | | | | |
|--------------|----|---------------|-------|-------|-------|-------|-------|-------------|-------|-------|-------|-------|-------|
| Added load | kg | 17,02 | 27,02 | 37,02 | 47,02 | 57,02 | 67,02 | 17,02 | 27,02 | 37,02 | 47,02 | 57,02 | 67,02 |
| Central Wing | mm | 2,86 | 5,13 | 7,27 | 9,1 | 10,35 | 15,15 | 3,236 | 5,138 | 7,039 | 8,941 | 10,84 | 12,74 |
| Half Wing | mm | 2,14 | 3,81 | 5,43 | 7,04 | 8,45 | 11,59 | 2,804 | 4,452 | 6,099 | 7,747 | 9,394 | 11,04 |
| Hull SX | mm | 2,78 | 4,95 | 7,08 | 8,68 | 8,94 | 14,02 | 3,46 | 5,493 | 7,526 | 9,559 | 11,59 | 13,63 |
| Hull DX | mm | 2,59 | 4,84 | 6,86 | 8,57 | 10,02 | 13,47 | 3,46 | 5,493 | 7,526 | 9,559 | 11,59 | 13,63 |
| Hull 2/3 SX | mm | 2,66 | 4,72 | 6,69 | 8,01 | 8,01 | 13,44 | 3,136 | 4,979 | 6,281 | 8,664 | 10,51 | 12,35 |
| Hull 1/3 SX | mm | 2,6 | 4,65 | 6,59 | 8,45 | 10,35 | 14,12 | 3,038 | 4,823 | 6,609 | 8,394 | 10,18 | 11,96 |

Table 6 - FEM and experimental displacement comparison

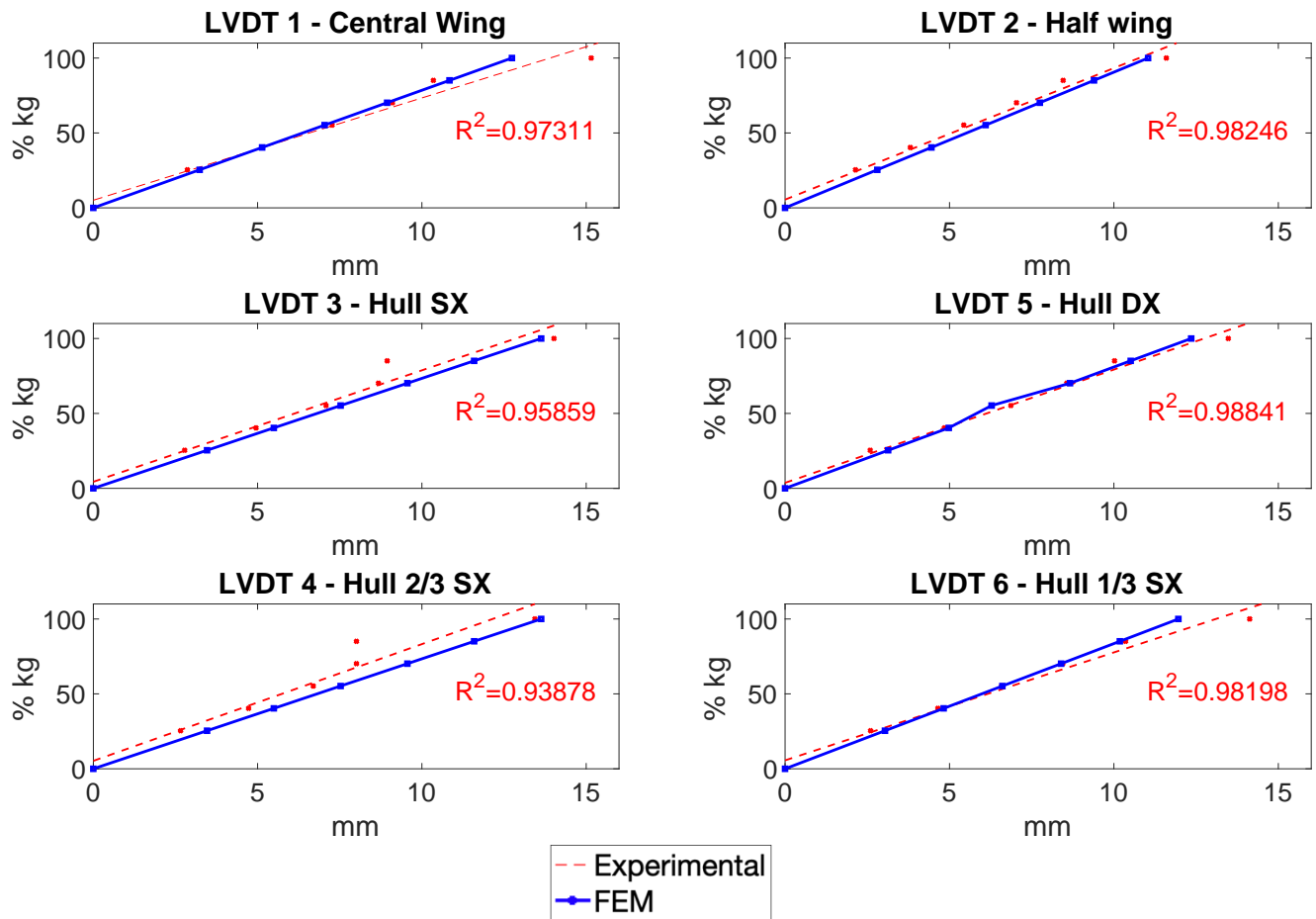


Figure 10 - Fem and Experimental Displacement measured

Table 6 and Figure 10 summarize the FEM displacement and experimental ones. Up to a load of 67.02 kg, the model aircraft had a slightly stiffer behavior than the FEM model.

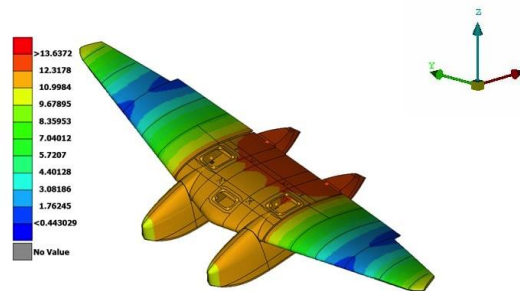


Figure 11 – Deformed model with displacement distribution

Figure 11 shows the results that were obtained inducing a load of 67.02 kg on the structure. The values of deformations and displacement that were obtained experimentally were close to the theoretical ones.

5. New Version of WST (Wing Static Test)

A more complete test was planned in order to collect more detailed data about the structure's behavior. In the complete form, deflections and strains were measured up to LL and UL conditions.

5.1. Loads

The loads that had to be simulated through the WST had been calculated in two steps: first, an analysis was performed on a longitudinal maneuver at a load factor condition of $N_z=4$ [6]. Three equilibrium equations were defined: vertical forces equilibrium with total lift, weight, and centrifugal force, horizontal forces equilibrium with total drag and total thrust, and finally, equilibrium of aerodynamic and propulsive pitching moment. Then, the produced data was used to perform an aerodynamic analysis with AVL. The definition of the wing loads along the wingspan, represented in Figure 12. To evaluate the equivalent load on the structure, a MATLAB code was written.

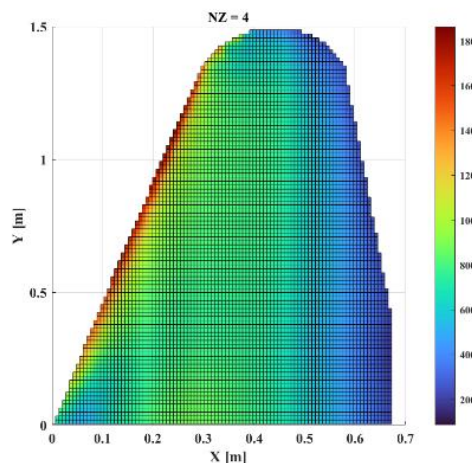


Figure 12 - Pressure distribution

An equivalent force was defined for each strip along the wingspan, and it was possible to obtain the external load to plot both shear and moment distributions.

The inertial load was defined considering a 4g acceleration on the mass distribution along the wingspan. It was possible to create the resulting real graphs using the equilibrium equation after the calculation of the applied load.

Constraints positions must be determined to create a realistic trend during the experimental test. A tree structure of load saddles was designed to replicate, in a static test, the real load condition of inertial and

aerodynamic loads. The constraints were applied through a lever system that was divided into three levels and were positioned in correspondence of three ribs for each half wing. An equivalent load on the hulls had to be used to simulate proper the maneuver, and it was equal to 404.16 N for each hull. Numeric values are reported in Table 7 with the respective rib wingspan coordinate.

| Ribs coordinate [m] | Reaction value [N] |
|---------------------|--------------------|
| 0.1045 | 29.15 (F1) |
| 0.5572 | 124.7 (F2) |
| 0.930 | 101.7 (F3) |
| 1.366 | 73.59 (F4) |

Table 7 - Constraint reactions

Figure 13 shows, with a dashed line, the real shear and bending moment, while the solid lines show the trend obtained applying the loads listed in Table 7. The dashed vertical lines identify the ribs' coordinates along the wingspan with the loaded ribs marked, the shear step on the second rib from the center is the inertial load of the hull.

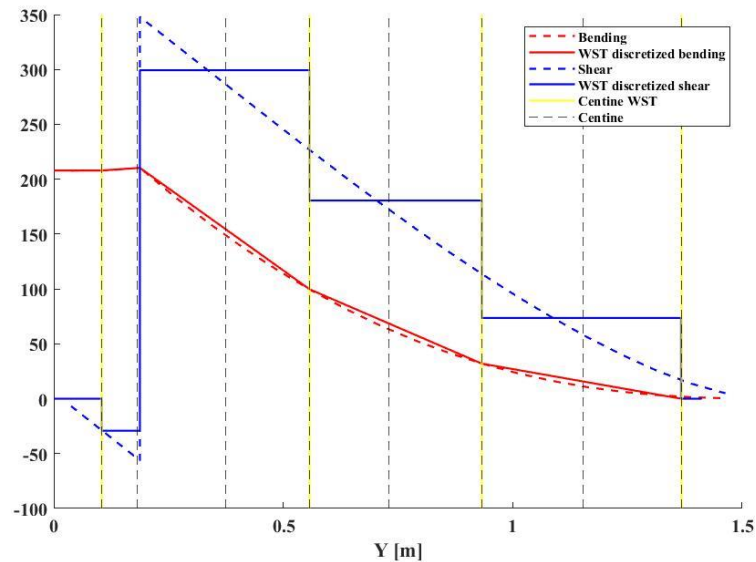


Figure 13 - Bending moment and shear stress trend

The sizing of leverage arms had to guarantee the moment equilibrium of the entire model aircraft during the test. Figure 14 is a more straightforward representation of the leverage system. The arms' dimensions were calculated through rotation equilibrium around each fulcrum and considering the distances between each rib, the results are shown in Table 8.

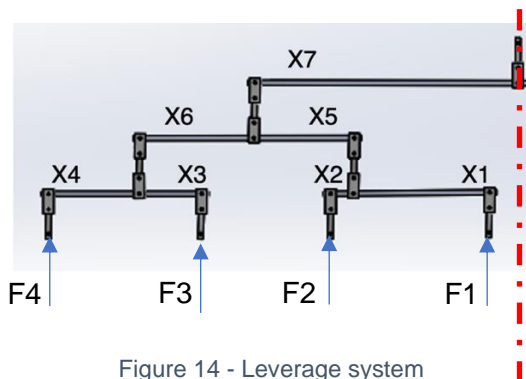


Figure 14 - Leverage system

| | | | |
|----|----------|----|----------|
| X1 | 0.388 m | X5 | 0.286 m |
| X2 | 0.0645 m | X6 | 0.324 m |
| X3 | 0.178 m | X7 | 0.7486 m |
| X4 | 0.258 m | | |

Table 8 - Leverage coordinate

To determine the attachment position on the wing's chord of the levers in the various ribs, the resulting global aerodynamics was considered. A resultant was obtained in a position corresponding to 48% of the aerodynamic chord at the plane of symmetry. Once the transverse coordinate was obtained, it was used as the point of application of the forces for all the other ribs.

| Ribs coordinate [m] | Chord length [mm] | Point of application of force [percentage of aero chord] | Resulting real rib aerodynamics [percentage of aero chord] |
|---------------------|-------------------|--|--|
| 0 | 691.44 | 48.0% | 48.0% |
| 0.1045 | 671.43 | 48.8 % | 43.9 % |
| 0.5572 | 549.82 | 40.2 % | 37.4 % |
| 0.930 | 428.13 | 32.6 % | 37.2 % |
| 1.366 | 162.17 | 26.7 % | 40.8 % |

Table 9 - Ribs coordinate with respect to the symmetric seaplane plane and Force resultant position

Table 9 lists the loaded ribs dimension and position and compares the actual position of the aerodynamic resultant on the section with the position of the loading tree.

5.2. FEM Analysis

Using the ANSA software from BETA CAE Systems, the experimental test was simulated as follows. Reference is made to the same model introduced in chapter 1. RBe2 type elements have been created for each rib, bringing together the lower nodes, those subject to the applied load. The RBe2 master was positioned on the upper area of the rib, at the point where it will then be connected to the leverage system. At that point, the force corresponding to the rib was then applied. An example is shown in Figure 15 for a rib.

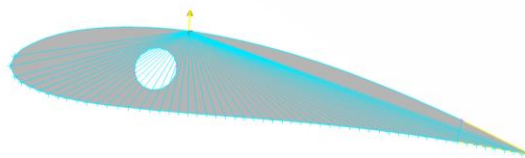


Figure 15 - Loading scheme example

The structure was constrained vertically (z direction) and transversely (x direction) in correspondence with the belts, and a longitudinal constraint (y direction) was inserted to eliminate labilities. We note how the applied forces are all at the same distance in the x-direction in Figure 16.

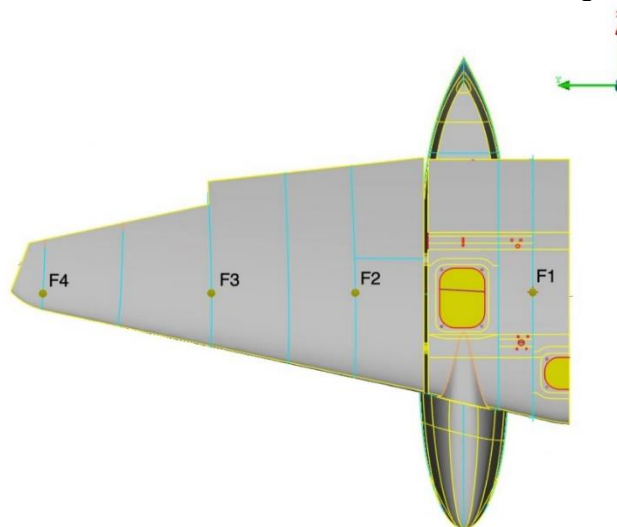


Figure 16 - ANSA symmetrical top view

The FEM maximum displacement obtained is 19.8 mm at the wingtip. The FEM highest stress values for skins and spars are also reported in the following figures. The strain gauges will be mounted during the experimental test in correspondence with the highlighted elements, in which the maximum deformation value was also recorded. The results obtained are shown in Figure 17, Figure 18, Figure 19.

0:5M01_WST_2022.op2 : Scalar: Displacements,Translational,Magnitude : : SUBCASE 1

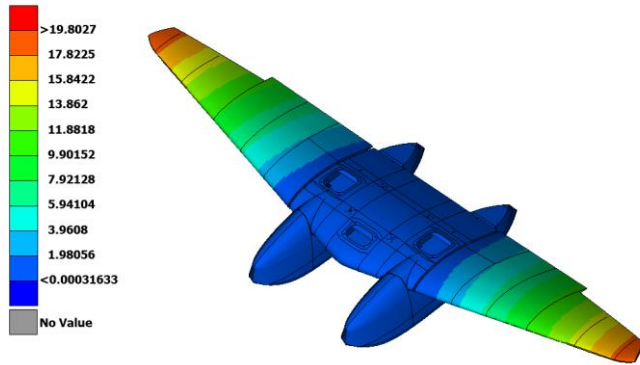


Figure 17 - Deformed experimental model with displacement distribution

0:WST2022.op2 : Scalar: Composite Stresses,Major Principal,Max of All Layers : : SUBCASE 1

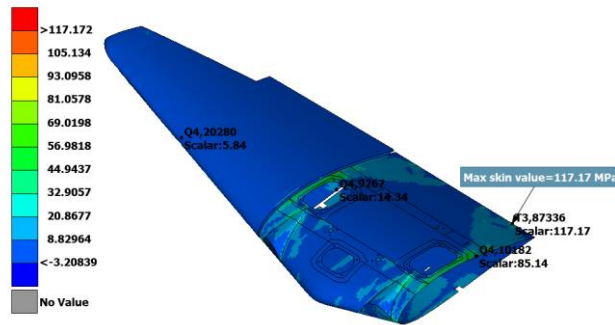


Figure 18 - Skin stress distribution

0:WST2022.op2 : Scalar: Composite Stresses,Major Principal,Max of All Layers : : SUBCASE 1

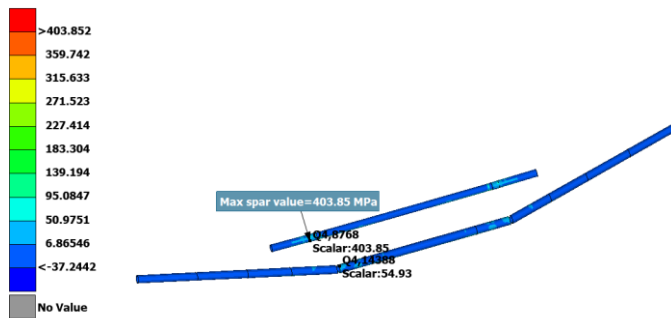


Figure 19 - Spars stress distribution

The most significant stresses were found in the spars and in the bayonet, used for the connection between the central wing box and half-wings. To validate the approximate positioning of the resultant, in Figure 20 the results were reported in terms of deformation that were obtained on the model with real aerodynamic loads.

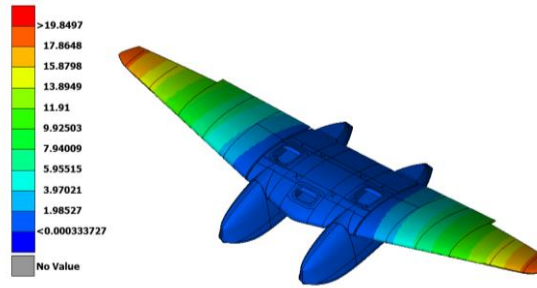


Figure 20 - Deformed real model

5.3. Instrumentation

5.3.1. Sensors

Four LVDT described in part 2.3.1 and four couples of strain gauges were chosen as sensors for this static test. They are shown in Figure 21 and described in Table 10. The strain gauges were attached in the same spot on both external surfaces of a component subject to bending. They are linked together to work as a single sensor. In this configuration, the strain gauges give a higher value of output. This lowered the effect of noise on the measurements.

| | | |
|----------------------------|-------------------------|---------------|
| Strain gauge model | | LY4 - 3/120 |
| A | Mm | 3 |
| B | Mm | 1.2 |
| C | Mm | 8 |
| D | Mm | 5 |
| Nominal (rated) resistance | Ω | 120 |
| Gage factor | | 1.95 \pm 1% |
| Maximum elongation | $\mu\text{m}/\text{mm}$ | \pm 50.000 |

Table 10 - Strain gauges model and data

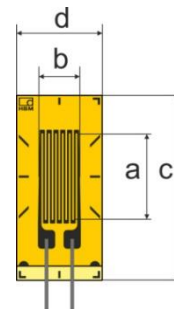


Figure 21 - LY4 strain gauge

The sensors were connected to the acquisition system HBM QuantumX MX840B and to a computer with the HBM Catman software to elaborate and save data.

5.3.2. Sensor placement

Displacement transducers were placed in spots 1, 2, 3, and 6 identified for the simplified test in Table 5 to verify the data consistency between the different procedures. Strain gauges were placed where the FE simulation results showed the most relevant strain values: Figure 22 are indicated on the CAD model in green the placement of strain gauges on the skin and in red the placement on the rear spar. The sensors were lined with the y axis of the seaplane, in Table 11 are the gauges positions referred to the plane axis of symmetry and to the section chord.

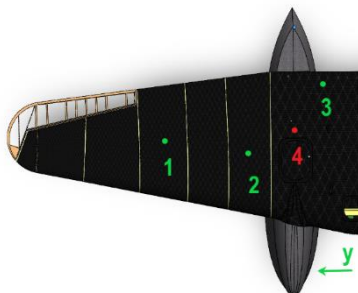


Figure 22 - Placement of strain gauges

| Gauge ID | Coordinate y (m) | % of chord (from Leading edge) |
|----------|------------------|--------------------------------|
| 1 | 0.85 | 50% |
| 2 | 0.45 | 38% |
| 3 | 0.15 | 85% |
| 4 | 0.25 | Rear Spar |

Table 11 - Strain Gauges positioning

5.4. Constraint system

5.4.1. Lever system

The design was based on the tree structure shown in Figure 23, which was divided into three levels connected by horizontal beams and vertical rods.

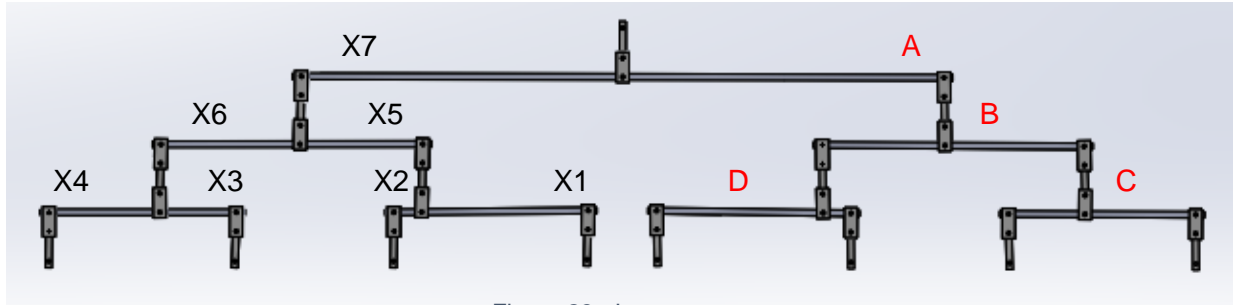


Figure 23 - Lever system

In Table 12, beams' lengths are reported. They were calculated using structural analysis to recreate the actual load, guaranteeing the proper distribution during the entire test. Levers' identification number and letter are shown in Figure 23 the letter represents the beam in its entire length, while the alphanumerical value indicates the segments' lengths that the central constraints create.

| Beam | Segment | Length [mm] |
|------|---------|-------------|
| D | X1 | 388 |
| | X2 | 64,5 |
| C | X3 | 178 |
| | X4 | 258 |
| B | X5 | 286 |
| | X6 | 324 |
| A | X7 | 748,6 |

Table 12 - Beams' lengths

In Figure 24 beams and rods' connection is showed.

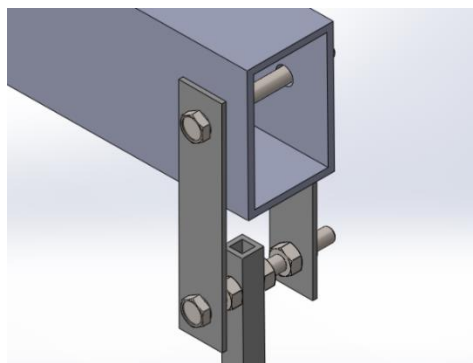


Figure 24 - Connections between parts

The fixed constraint was guaranteed by connecting the lever system to the ceiling.

The material for the structure's beams and their geometry were chosen according to the operative conditions. Each beam was sized in order to limit the deformation (w) at 5 mm max.

Imposing this requirement when the structure was loaded with LL and a 150 MPa as allowable stress, beams' geometry was identified in rectangular tubes sized as in Table 13:

| | h x b x t | Unit |
|---------------|------------------|-------------|
| Beam A | 60 x 40 x 3 | mm |
| Beam B | 40 x 20 x 2 | mm |
| Beam C | 30 x 15 x 1,5 | mm |
| Beam D | 20 x 10 x 1,5 | mm |

Table 13 - Beams' sections

Section's geometry is shown in Figure 25.

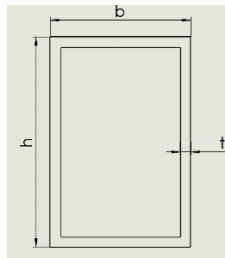


Figure 25 - Section's geometry

The vertical bars and the plates were sized after traction resistance, finding the geometry shown in Table 14.

| | b | h | t | Unit |
|-----------------------|----------|----------|----------|-------------|
| Plates | 20 | / | 3 | mm |
| Vertical Beams | 10 | 10 | 2 | mm |

Table 14 - Plates and Vertical beams' geometry

5.4.2. Saddles

The lever system was connected to the seaplane by wooden saddles, which were symmetrically positioned on the inner rib of the central wing box and on the second, fourth, and sixth ribs of the half-wing, as represented Figure 26.

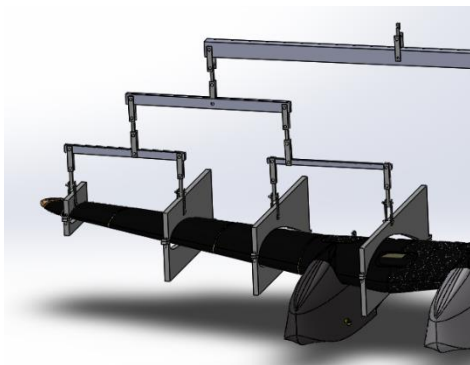


Figure 26 - Half wing in the final configuration

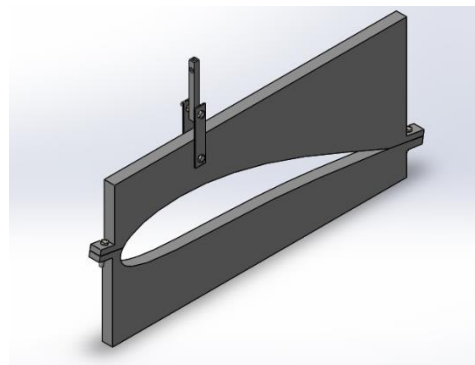


Figure 27 - Wooden saddle

Figure 27 shows the saddles, which were shaped like the ribs they were clamped to.

5.5. Procedure

The Test Article was the same as part 2. Each hull weighs 5.15kg, that is equivalent to 404.16 N in the Ultimate Load configuration.

However, the bending's discretization determined a different shear's value. Consequently, shear's discontinuity, which is generated by the hull, is about 328 N.

The Limit Load condition was reached by adding weight in four discrete steps of 2kg until the total equivalent load of 33kg will be reached.

Ultimate Load test followed similar loading procedure with 4 steps of 2kg, one step of 3 kg and five of

6kg to reach the total ultimate load of 66kg.

The two tests had the same aim: they wanted to evaluate the seaplane's displacement and deformation. Table 15 summarizes both the Limit Load and Ultimate Load the load steps.

| | Limit Load – LL | | Ultimate Load - UL | |
|---------|-----------------|------|--------------------|------|
| | Eq. Load (kg) | %LL | Eq. Load (kg) | %UL |
| Step 0 | 25 | 76% | 25 | 76% |
| Step 1 | 27 | 82% | 27 | 82% |
| Step 2 | 29 | 88% | 29 | 88% |
| Step 3 | 31 | 94% | 31 | 94% |
| Step 4 | 33 | 100% | 33 | 100% |
| Step 5 | \ | \ | 36 | 109% |
| Step 6 | \ | \ | 42 | 127% |
| Step 7 | \ | \ | 48 | 145% |
| Step 8 | \ | \ | 54 | 164% |
| Step 9 | \ | \ | 60 | 182% |
| Step 10 | \ | \ | 66 | 200% |

Table 15 - Load steps for LL and UL Test

6. Conclusions

In this document, the results of the *Wing Static Test* are described; it was performed by installing the model on a pair of constraints and the load on the hulls. The final result was satisfactory, so we decided to proceed with the seaplane flight test program made by “Politecnico di Torino” in Team S55.

The model aircraft studied in this document had a more rigid behavior than expected until it reached a load of 67.02 kg, as shown in Figure 10. The reason can be attributable to the material used to make the seaplane, such as putty and glue. These were also included in the FEM model as a non-structural mass, therefore not helpful in increasing their structural stiffness.

The results presented in this document are a good starting point for executing the more complex and complete version of the *Wing Static Test* described in paragraph 5.

7. Contact Author Email Address

The corresponding author can be contacted at the following email addresses: enrico.cestino@polito.it

8. Copyright Statement

The authors confirm that they, and/or their company or organization, hold copyright on all of the original material included in this paper. The authors also confirm that they have obtained permission, from the copyright holder of any third party material included in this paper, to publish it as part of their paper. The authors confirm that they give permission, or have obtained permission from the copyright holder of this paper, for the publication and distribution of this paper as part of the ICAS proceedings or as individual off-prints from the proceedings.

9. References

- [1]. Di Ianni L¹, Loiodice L¹, Celestini D¹, Tiberti D¹, Baldon C¹, Iavecchia P¹, Saponaro Piacente A¹, Prodan M¹, Grendene S¹, Barberis B¹. and Santoro L¹, ¹Politecnico di Torino, Italy, Team S55: 1:8 scale “replica” of the SIAI-MARCHETTI S55-X, *Proc of 32nd ICAS 2018 Congress*, 6-10 September 2021, Shanghai (China)
- [2]. Cestino E¹, Frulla G¹, Sapienza V¹, Pinto P¹, Rizzi F¹, Zaramella F.¹ and Banfi D. ¹ REPLICA 55 PROJECT: a wood seaplane in the era of composite materials, *Proc of 31st ICAS 2021 Congress*, 9-14 September 2018, Belo Horizonte (Brasil)
- [3]. JAR 25.301 - Loads
- [4]. JAR 23.305 - Strength and Deformation
- [5]. Frulla G. ¹ and Cestino E. ¹ Design, manufacturing and testing of a HALE-UAV structural demonstrator, *Composite Structures*, Vol. 83, No. 2, pp. 143-153, 2008
- [6]. Baldon C¹, Indelicato R¹, Bottino N¹, Sinisi M¹, Carrone F¹, Cantanna G¹, Cestino E¹. and Sapienza V. Aeronautical Consultant S55 Project, ¹Politecnico di Torino, Italy, CFD Analysis of an historical seaplane, *Proc of 32nd ICAS 2018 Congress*, 6-10 September 2021, Shanghai (China)

We would like to thank the Politecnico di Torino which has been supporting the team financially since 2017, investing in our projects. Thanks to all the companies and organizations that collaborate with the Team S55: Replica 55, Ellena-SPEM, BETA CAE Systems, Altair Engineering, HPC Polito, Siemens, Mike Compositi, Ades Group, MODLab Design, and Erre ti Compositi. Eventually, the authors thank Giuseppe Marinacci who collaborated to the review of the paper.